J Mater Sci (2008) 43:55–63
DOI 10.1007/s10853-007-2077-9

An investigation of the densification and microstructural evolution of M2/316L stepwise graded composite during co-sintering

V. Firouzdor · A. Simchi · A. H. Kokabi

Received: 14 May 2007 / Accepted: 31 July 2007 / Published online: 27 September 2007

Abstract The densification and microstructural evolution during co-sintering of M2 tool steel/316L stainless steel composite layers with and without boron addition was studied. A pressureless sintering method in conjunction with a powder layering technique was used to fabricate the stepwise graded composite layers. Isothermal and non-isothermal sintering response of the individual and composite layers was examined and the microstructural features of the bonding zone were studied. Shear strength and microhardness of the bonding zone were also measured. It was shown that an enhanced densification is obtained in the composite layers due to (i) sintering shrinkage incompatibility between two steels, (ii) interlayer diffusion of the alloying elements and formation of a dual δ-ferrite/austenite phase at high temperature, and (iii) formation of a low temperature eutectic Fe (C)-B phase at the interface in the samples containing boron. The morphology of carbides in M2/316L is significantly changed as the sintering temperature increases, i.e., they appeared as fine intergranular carbides at low temperatures (1,240 °C), thick film at 1,260 °C and herringbone shape eutectic at 1,290 °C. Elongated grains with an intergranular boride phase were seen in the bonding zone of M2/316L + B layers. The shear strength of the interface of the composite layers was found to be superior to that of the individual layers.

V. Firouzdor · A. Simchi (✉) · A. H. Kokabi
Department of Materials Science and Engineering, Sharif University of Technology, P.O. Box 11365-9466, Azadi Avenue, Tehran 14588, Iran
e-mail: simchi@sharif.edu

A. Simchi
Institute for Nanoscience and Nanotechnology, Sharif University of Technology, P.O. Box 11365-9466, Azadi Avenue, Tehran 14588, Iran

Introduction

Functional grading of components requires the design and fabrication of two or more material systems whose combination endow unique properties, specific to desired applications. An example is the production of high hardness and wear resistance tool steels with a stainless steel. Such a combination of toughness, corrosion, and wear resistance yields advantages over components made from tool steels. According to prior art, such combination has to be made by welding processes. The addition of a secondary joining operation has the disadvantages of higher cost, need to an extra manufacturing step, and additions of a third (weld-) material different from the base materials [1]. An obvious improvement over welding or similar approaches is to sinter two materials to one piece while they have contact to each other, i.e., co-sintering [2, 3]. For this purpose, it is necessary that the two materials follow a similar shrinkage pathway to avoid development of mismatch stresses at the interface which may lead to cracking, warpage, or distortion. The interlayer diffusion of alloying elements and formation of undesired phases must also be taken into account. Hence, the sintering step is the key stage in the manufacturing route.

This article presents the densification response and microstructural features of M2 tool steel and 316L stainless steel powders during co-sintering. In the previous work, co-sintering of 17-4PH/316L stainless steels [4], 728/618 Inconel alloys [5], 3Y-TZP/stainless steels [6], and Co-Cr-Mo F-75 alloy with different particle size [7] for

fabrication of stepwise graded composite layers have been presented. Fabrication of magnetic/non-magnetic micro-parts by co-injection molding of 17-4PH, Fe, and 316L has also been reported [8]. An approach for assessment of the co-sintering behavior by using dilatometric analysis has been presented in [9]. So far, a little work has been performed on co-sintering of tool steels with low alloy and stainless steels. Pest [10] has examined the co-sintering of M4 and Fe2Ni1B steels and has found that significant differences exist in sintering behavior, so a sound part cannot be fabricated. Heaney et al. [3] have reported the co-sintering of M2 tool steel and 4340, Fe–10Cr, Fe2Ni, and 316L steels. They have found that with the addition of 0.5%B and adopting suitable sintering parameters, defects-free components can be obtained in M2/316L combination. No detailed results on the microstructural features of the sintered parts, particularly with respect to interlayer diffusion of the alloying elements and reaction between them to form borides and carbides have been described. In addition, the strength of the bonding zone has not been examined. The aim of the present work is to extend the knowledge of densification and microstructural development in M2/316L system containing boron.

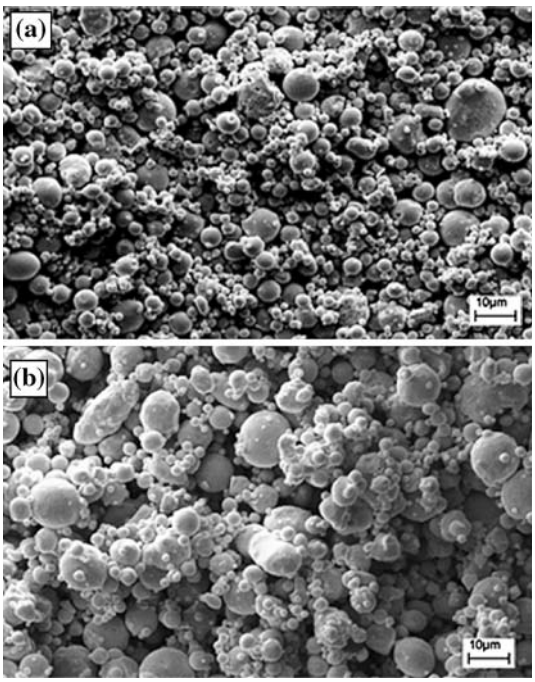

Fig. 1 SEM micrographs show the particle morphology of M2 (**a**) and 316L (**b**) powders

Experimental procedure

Commercially available gas atomized M2 high speed steel (HSS) and stainless steel (SS) powders were supplied by Osprey Co., UK. The chemical composition of the powders is typical for M2 HSS and 316L SS with the characteristics given in Table 1. The powder particles are almost spherical, which is typical for their method of production, i.e., gas atomization (Fig. 1). Amorphous boron powder (Merck, Germany) was used as an additive to 316L SS at the amount of 0.2 and 0.5 wt% with the aim of enhancing the sintering response via formation of Fe-B liquid phase. A Turbula T2C (Basle, Switzerland) shaker was used to blend the 316L + B mixture for 40 min.

The sintering response of the powders was studied either by isothermal sintering in a batch laboratory furnace or non-isothermal sintering in a dilatometer (TMA 801, Netzsch, Germany). In the all experiments, the heating and cooling rate was 5 and 10 K min^{-1}, respectively. A reducing atmosphere containing 20 vol% H_2 mixed with Ar was used. The same sintering cycle was applied to the stepwise composite layers of M2/316L and M2/316L + B. An alumina tube with 12 mm diameter was used as a mold. About 2 g of the M2 powder was poured in the alumina tube and the die was slightly tapped to spread the powder evenly at its bottom. Light pressure was applied (by hand) to flatten that layer. Subsequently, about 2 g of the 316L SS powder was poured on top of the flattened M2 layer. Once again, the die was lightly tapped and pressed. The sintering temperature was between 1,220 and 1,320°C and the holding time was 90 min.

The density of the sintered samples was measured by the water displacement method (Archimedes method). For microstructural evaluation, the sintered parts were sectioned in the direction of the hand pressing. The sample preparation for metallographic study was performed according to the standard method of grinding on emery papers and subsequently alumina polishing. Fry's (5 g $CuCl_2$, 40 mL HCl, 30 mL H_2O, and 25 mL ethanol) reagent was used for chemical etching. A scanning electron microscope (TE Scan Vega 2XMU SEM, Czech Republic)

Table 1 Characteristics of powders used in this study

Powder	Chemical composition (wt%)	Tap density (g cc^{-1})	Theoretical density (g cc^{-1})	D_{10} (μm)	D_{50} (μm)	D_{90} (μm)
M2	6.3W–4.9Mo–4.2Cr–2V–0.91C–0.24Si	5.0	8.2	4	12	22
316L	17.3Cr–12Ni–2.3Mo–1.2Mn–0.45Si–0.019C	4.7	7.9	4	8	16

coupled with EDX analysis as well as optical microscope (OLYMPOUS PME3, Japan) were employed for microstructural study. To measure the interface shear strength, a special clamp was designed and built to fix the composite layer. Then, a shear force was applied by using an Instron-6027 tensile test machine at the cross speed of 2 mm/min. The hardness of the sintered layers was evaluated by a HVM-2000 Shimadzu micro-hardness tester at a load of 100 g.

Results and discussion

Densification

In Table 2, the sintered density of individual and composite layers after isothermal sintering at different temperatures is reported. Figure 2 shows the non-isothermal sintering behavior of the powders. The comparative dilatometer data are summarized in Table 3. Based on the experimental results, the following findings can be enumerated.

- Sintering temperature has a profound effect on the densification of M2 HSS and 316L layers, i.e., the density increased significantly with increasing temperature. The influence of sintering temperature on the densification of M2 is more pronounced as compared with 316L; a significant densification was noticed when the tool steel turned mushy at 1,260 °C.
- The sinterability of M2 HSS seems to be higher than that of 316L SS. As Fig. 2 shows, both powder starts to shrinkage at relatively low temperature of 931 °C (Table 3). M2 HSS exhibited a sharp shrinkage rate at 1,239°C while 316L showed diffusive shrinkage rate peak at 1,024 and 1,197°C. The difference between the sintering responses of the powders enables to induce mismatch shrinkage upon sintering, which is undesirable.

Table 2 Density (%theoretical) of individual and composite layers after sintering at different temperatures for 90 min in Ar + 20vol%H_2 atmosphere

Temperature (°C)	1,220	1,240	1,260	1,290	1,320
M2	86	91.7	94.7	97.1	97.6
316L	76	84.4	87.2	91.1	95
316L + 0.2B	86.5	92	–	–	–
316L + 0.5B	92.5	94.2	93.6	89.2	–
M2/316L	83.4	87.6	91.3	96.4	96.5
M2/316L + 0.2B	90.2	92	–	–	–
M2/316L + 0.5B	92.3	94	94.5	91.3	–

The heating and cooling rate was 5 and 10 K min^{-1}, respectively

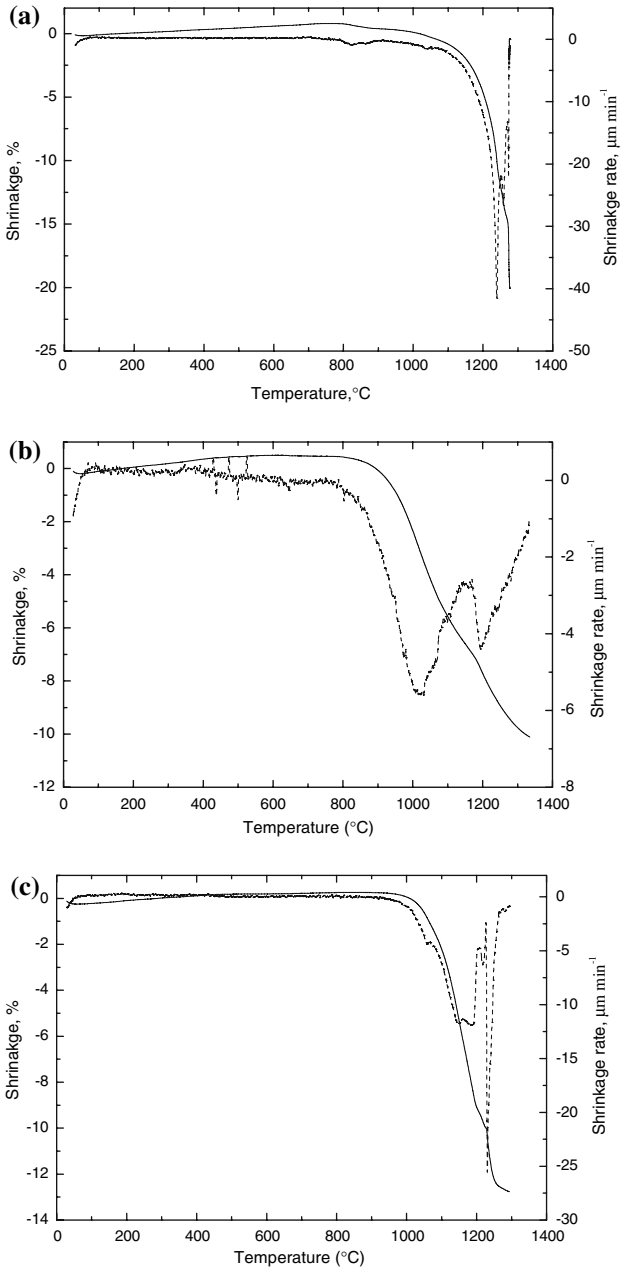

Fig. 2 Dilatometric curves of M2 (**a**), 316L (**b**) and 316L + 0.2 wt%B (**c**) powders. The solid and dash lines show shrinkage and shrinkage rate, respectively

- Addition of boron to 316L significantly enhanced the sintering response at relatively low sintering temperatures of 1,220–1,260 °C. The density of 316L + 0.2B is close to M2 after sintering at 1,240°C (~92% theoretical, TD) which is desirable. The sintering shrinkage is enhanced at the higher B concentration (0.5 wt%), but part distortion and slumping at $T > 1{,}260$ °C due to excess liquid phase reduced the final density. The dilatometric curve of boron added SS (Fig. 2c) exhibits a high shrinkage rate at 1,239 °C.

Table 3 Dilatometry data of the used powders

Powder	$T_{0.5}$ (°C)	T (°C) (Peak 1)	ε (%) (Peak 1)	T (°C) (Peak 2)	ε (%) (Peak 2)	T (°C) (Peak 3)	ε (%) (Peak 3)
M2	931	1,239	10.1	1,258	13.3	1,274	16.7
316L	931	1,024	3.2	1,197	7.6	–	–
316L + 0.2 wt%B	1045	1,041	1	1,145	4.9	1,231	10.4

$T_{0.5}$: temperature at 0.5% shrinkage; T: temperature at the shrinkage rate peak;
ε: amount of strain at T

- In consistency with the density of individual layers, sintering temperature has a profound effect on the densification of composite layers. Nevertheless, it was noticed that the sintered density of the composite layer is not always compromise of the density of each counterparts. In other words, the density of bilayers does not obey the "rule of mixture" that is the average of the density of the individual layers. The difference between the actual density of the bilayers and the average density calculated according to the rule of mixture is named excess densification. As Fig. 3 shows, the positive excess densification values indicate an improvement in densification with respect to the individual layers upon co-sintering.

Microstructure

Figure 4 shows the polished sections of sintered bilayers at different temperatures. A relatively dense band at the bonding zone of all layers was noticed while the outer regions were porous. The width of the band zone was found to be significantly increased with the boron addition and increasing the sintering temperature. Boron addition also resulted in the formation of elongated grains at the interface area (Fig. 4e). In this case, high temperature sintering at 1,290 °C caused the formation of a porosity band close to the 316L interface (Fig. 4f).

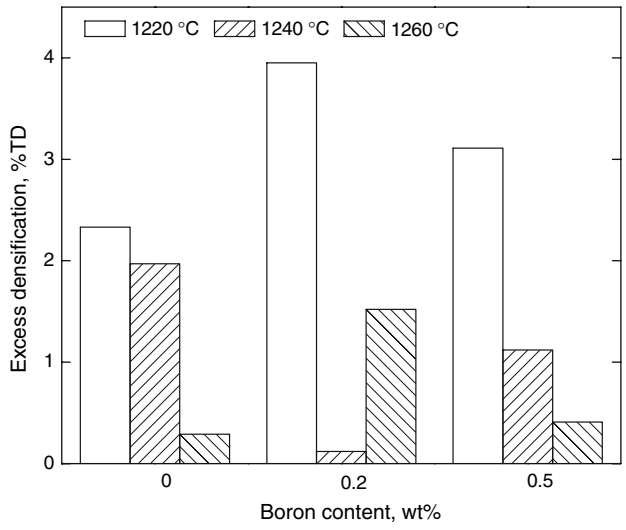

Fig. 3 Difference between the density of composite layers and the average density of the individual layers as a function of boron content and sintering temperature

Figure 5 shows SEM images of carbide morphology in M2/316L and M2/316L + 0.5B layers sintered at different temperatures. The microstructure of sintered M2 typically composed of martensite matrix plus retained austenite together with M_6C carbides [11, 12]. At 1,260 °C, the carbides appeared as small spherical particles within the grains or as big angular carbides at the prior austenite grain boundaries (Fig. 5a). By increasing the temperature, the morphology of carbides changed significantly; at 1,260 °C, the carbides appeared as thick elongated films at the grain boundaries (Fig. 5b), whereas at 1,290 °C herringbone shape eutectic carbides were observed (Fig. 5c). When boron was added, precipitation of a eutectic boride phase along the grain boundaries and fine intergranular carbides were noticed (Fig. 5d and e).

Figure 6 shows the microstructure of sintered layers after chemical etching. Since Fry's regent does not attack the austenite grain boundaries [13], the revealed microstructure of M2 helps the eyes to distinguish the interface boundary. In order to determine what the constitutional phases of the interface zone are, one can use Schafler diagram [14] by relinquishment of the effect of carbon. Figure 7a shows the results of lie scan EDX analysis throughout the boundary region in M2/316L specimen sintered at 1,240 °C as an example for Ni, Cr, Mo, and V due to their high concentration gradient. It appears that diffusion of Ni and Cr form 316L toward M2 layer and diffusion of Mo and V in opposite direction occurred. So, the interface region should contain ferrite + austenite + martensite + carbide phases as the amount of ferrite stabilizers increase. With increasing the sintering temperature, the diffusion of the alloying elements is faster, thus more ferrite phase was formed. In the Boron added layer, the interface layer appeared as a wide band with elongated grains (Fig. 6c). As an example, results of EDX lines scan analysis for Ni diffusion is shown in Fig. 7b. The data

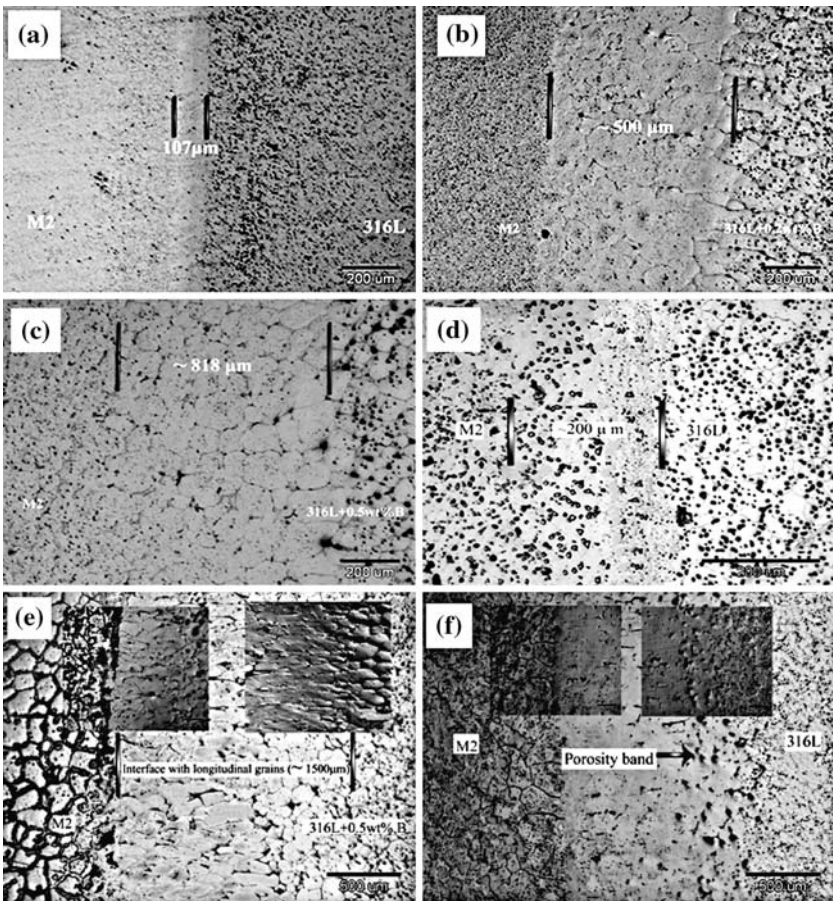

Fig. 4 Optical micrographs show the polished section of M2/316L sintered at 1,240 °C (**a**), M2/316L + 0.2B sintered at 1,240°C (**b**), M2/316L + 0.5B sintered at 1,240 °C (**c**), M2/316L sintered at 1,260 °C (**d**), M2/316L + 0.5%B sintered at 1,260 °C (**e**), and M2/316L sintered at 1,290 °C (**f**)

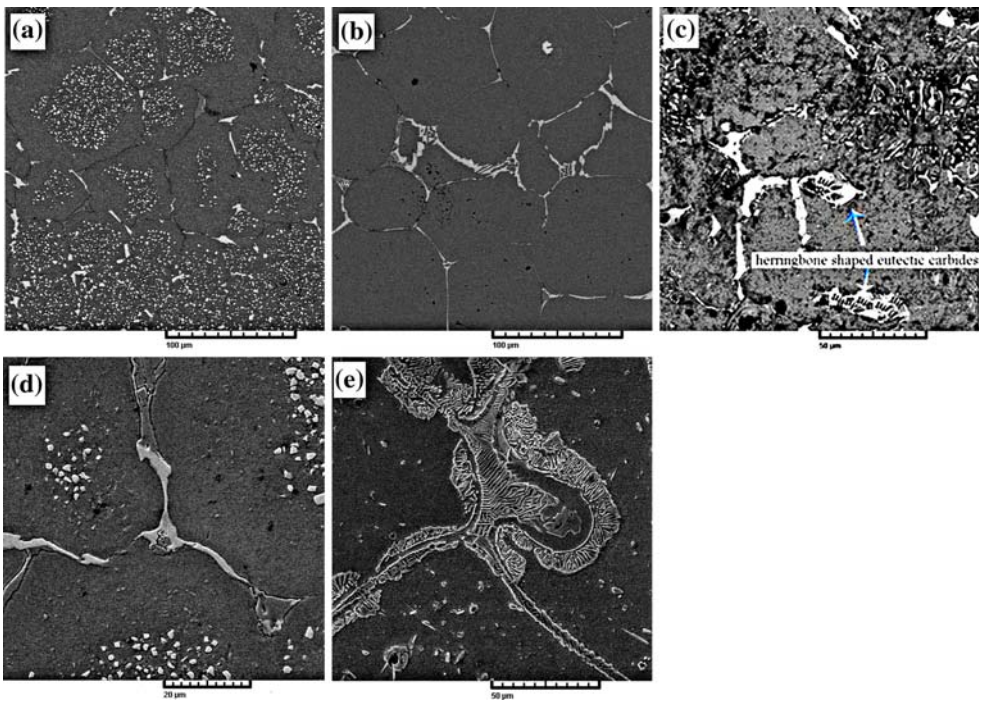

Fig. 5 SEM micrographs show the morphology of carbides in M2/316L (**a**, **b**, **c**) and M2/316L + 0.5B (**d**, **e**). Sintering temperature was 1,240°C (**a**, **d**), 1,260 °C (**b**, **e**), and 1,290 °C (**c**)

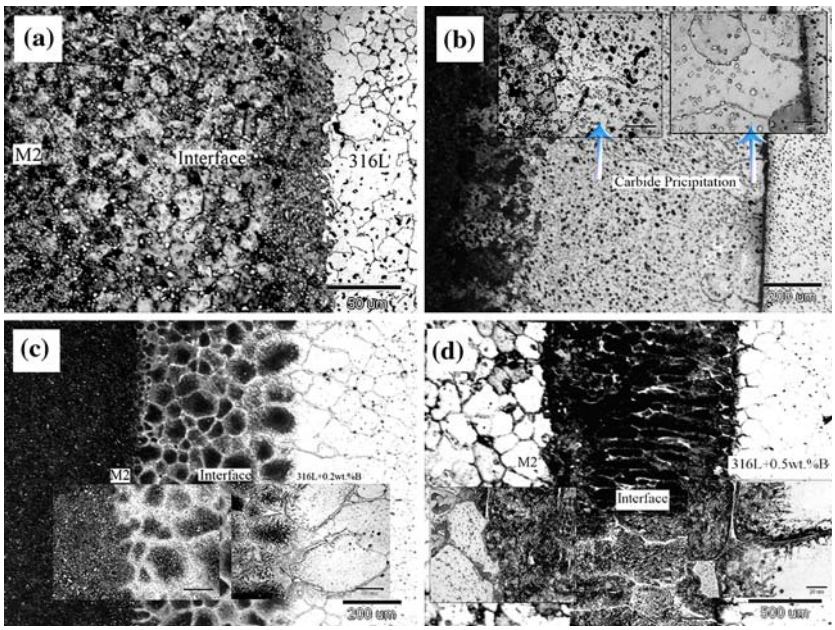

Fig. 6 Optical micrographs show the etched sections of M2/316L sintered at 1,240 °C (**a**), and 1,260 °C (**b**), M2/316L + 0.2B sintered at 1,260 °C (**c**), and M2/316L + 0.5B sintered at 1,260 °C (**d**)

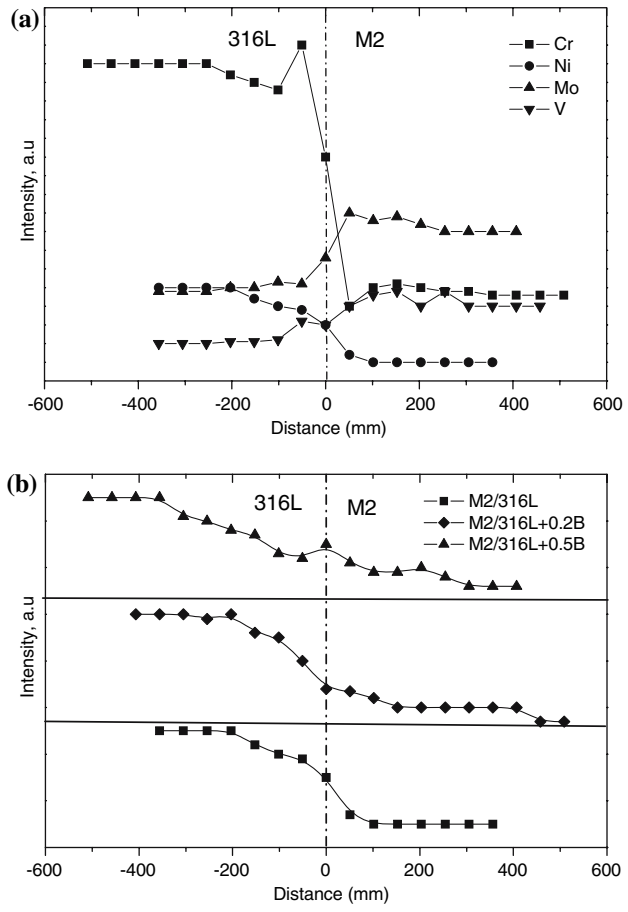

Fig. 7 EDX analysis of composite layers sintered at 1,240 °C: (**a**) Diffusion profile of alloying elements; (**b**) Ni profile dependent on the boron content

indicate that boron eases the diffusion process, so the diffusion affected zone was broadened. The microstructure mainly consisted of martensite + ferrite + austenite + carbide + boride phases.

Mechanical properties

Figure 8 shows the variation of hardness throughout the bonding zone. The dash vertical line corresponds to the Motano interface. In sintered M2/316L layer at 1,240 °C, a step change in the hardness value within 0.5 mm below the Motano interface is seen. The width of this zone increased with increasing temperature. For instance, it reached to

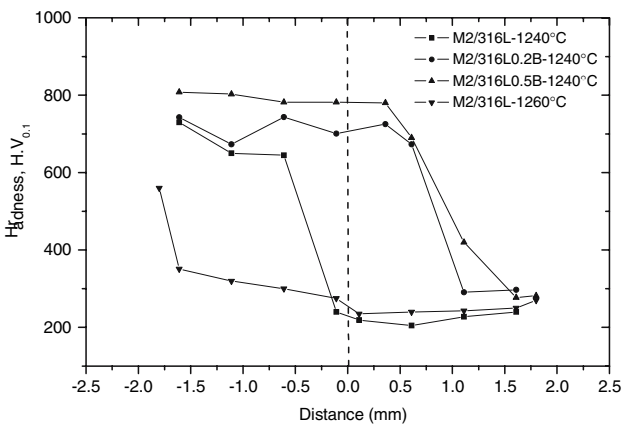

Fig. 8 Variation of hardness along the bonding zone of the composite layers

Table 4 Shear strength (MPa) of the individual layers and the bonding zone of the graded composite

Sintering Temperature (°C)	M2	316L	316L + 0.2B	316L + 0.5B	M2/316L	M2/316L + 0.2	M2/316L + 0.5B
1240	200	313	299	470	377	448	348
1260	347	414	*	475	465	*	437

* Not measured

2 mm after sintering at 1,260 °C. In this region, the hardness of matrix is lower due to the formation of ferrite phase. When Boron was added, a significant increase in the hardness compared with M2/316L was noticed. The step change in the hardness values was also shifted toward the 316L region.

The shear strength of the individual layers and the interface of bilayers are reported in Table 4. One can notice that the shear strength of the interface zone is higher than that of both 316L and M2 individual layers. The positive influence of boron addition and higher sintering temperature on the bond strength is also seen. Figure 9 shows representative SEM micrographs from the fracture surface of the sheared specimens. In the M2/316L layer, elongated dimples and microvoids are observed (Fig. 9a). In contrast, the fracture surface of the M2/316L + 0.5B layer exhibits inter-grain-boundary fracture characteristics.

Discussion

It was found that the densification response of M2/316L graded composite layer is slightly higher than that of the individual M2 and 316L layers, i.e., an enhanced sintering kinetics was observed upon co-sintering (Fig. 3). One possible explanation relates to the difference in shrinkage rate of the two layers during sintering. It is suggested that mismatch shrinkage develops stresses at the interface area, which may contribute on the densification. Figure 10 shows the shrinkage and shrinkage rate incompatibility between the M2 and 316L steels occurring upon non-isothermal sintering. The presence of biaxial mismatch stresses at the bonding zone, exerts an additional energy for densification as similar to the pressure assisted sintering, i.e., the internal pressure becomes operative in closing the

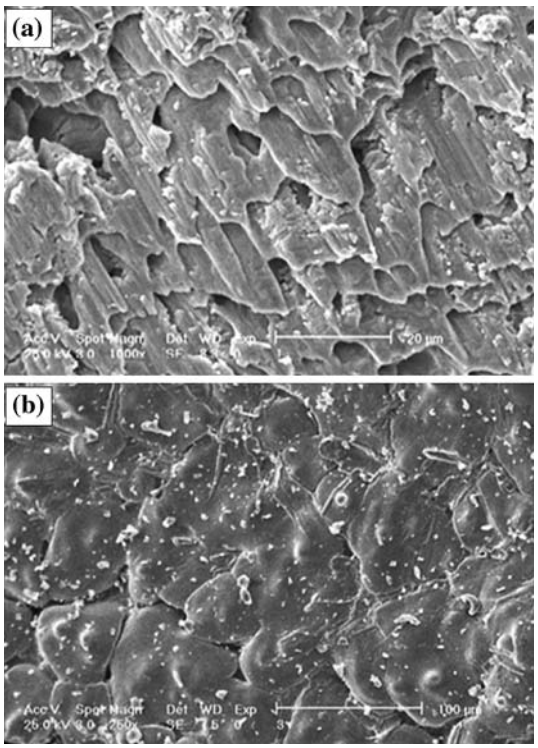

Fig. 9 SEM images show the fracture surface of shear-tested specimens sintered at 1,240 °C: (**a**) M2/316L; (**b**) M2/316L + 0.5B

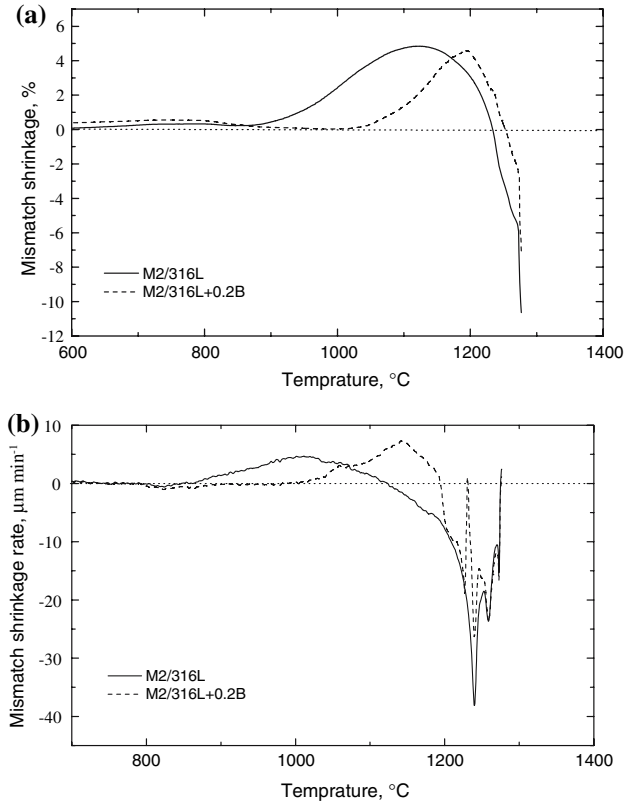

Fig. 10 Mismatch shrinkage (**a**) and shrinkage rate (**b**) between M2 and 316L steels during non-isothermal sintering

pores and densifies the powders. Here, it is important to note that one of the layers would be primarily in tension while the other would be in compression. Therefore, depending on the stress mode, the densification may be enhanced or hindered. The interlayer diffusion of alloying elements can also come to play a role. The interface plane movement due to the interlayer diffusion is accompanied by the formation of voids and development of tensile and compression biaxial stresses [15]. By comparison of the diffusion of the alloying elements, it is found that elements like Ni and Cr have higher diffusion coefficient in steels compard with elements that diffuse in the opposite side like Mo, V, or W due to their lower melting points and atomic volumes. So, it can be deduced that vacancies are created near the 316L part. Developments of biaxial compression in 316L layer, where vacancies are created, contribute in densification whilst the biaxial tension in M2, where vacancies are destroyed, decreased the densification rate [16]. In addition, diffusion of ferrite stabilizers, i.e., V and Mo, along the interface can contribute to the densification of 316L due to the formation of more ferrite phase during sintering. Shu et al. [17] have reported that Mo promotes the densification of 316L powder because of formation of dual-phase δ-ferrite/austenite with a higher diffusion rate. Increasing the sintering temperature enhances the diffusion depth, hence, the bonding zone becomes wider. The fracture surface of the bonding zone indicated microvoid coalescence, which is also an indicator of the presence of a soft (ferrite) phase at the interface.

When boron was added to 316L, another important factor contributes in the densification. As the dilatomery data showed, the development of mismatch shrinkage (stress) is shifted to higher temperatures (about 80 °C). Since the elastic modulus of the steels is lower at higher temperatures, it can be deemed that lower mismatch shrinkage would be developed upon processing. On the other hand, formation of a liquid phase due to the presence of boron creates a rapid diffusion pathway for the elements (for example, see Fig. 8b for Ni). Reaction between boron and Fe–C melt also results in the formation of a low-melting point, eutectic melt at the bonding zone, which can fill the pores and densifies the interface rapidly. The intergrain-boundary fracture mode of the shear-tested specimens is attributed to the formation of brittle boride phase [18] as well as martensitic matrix formed by deep diffusion of carbon along the interface as it was noticed in the hardness variation along the interface (Fig. 8).

Conclusion

Stepwise graded M2/316L composite layer was produced by pressureless sintering method in conjuction with a simple powder layering technique. The findings can be summarized as follows:

- Sintering response of metal injection moulding grade of M2 HSS is superior to 316L SS, i.e., the maximum shrinkage rate occurs at a lower temperature. The difference in the sintering shrinkage causes biaxial stress at the bonding zone, influencing the densification.
- The density of composite layer is higher than that of the average densification of individual layers at the same sintering temperature, which can be attributed to the mismatch sintering shrinkage and interlayer diffusion of alloying elements.
- Microstructural study of sintered M2/316L revealed that a dense band was formed at the interface. With increasing the sintering temperature the width of this band increases. Due to the interlayer diffusion, a dual δ-ferrite/austenite phase can be formed during sintering, which affects the densification of the bonding zone. The morphology of the carbides is changed from fine intergranular to thick film and herringbone shape eutectic at the grain boundaries with increasing the sintering temperature.
- Addition of boron to 316L powder increases the sintering response, leading to shifting of maximum mismatch shrinkage in M2/316L + B composite layer to higher temperatures compared with M2/316L. Better compatibility with M2 HSS was achieved by adding 0.2 wt% B to 316L.
- Formation of low melting point eutectic Fe (C)–B at the interface significantly contributes to the densification. The liquid improves the diffusion rate of the alloying elements along the interface. The microstructure of the interface consists of martensite, austenite, ferrite, and intergranular boride phases.
- The strength of the bonding zone in the composite layers was found to be superior to that of the individual layers. Microvoid coalescence and intergranular fracture modes were observed at fracture surfaces of the shear-tested M2/316L and M2/316L + B specimens.

References

1. Tan LK, Baumgartner R, German RM (2001) In: Advances in powder metallurgy and particulate materials, vol 4. Compiled by W.B. Eisen and S. Kassam, Metal Powder Industries Federation (MPIF), Princeton, NJ, p 191
2. Alcock JR, Logan PM, Stephenson DJ (1998) Surf Coat Technol 105:65
3. Heaney DF, Suri P, German RM (2003) J Mater Sci 38:1
4. Simchi A, Rota A, Imgrund P (2006) Mater Sci Eng 424 A:282
5. Simchi A (2006) Metal Mater Trans 37A:2549
6. Tamjid E, Simchi A, Hartwig T (2006) In: Proc. of the First Conference on Nanoscience and Nanotechnology. University of Tehran, Tehran

7. Dourandish M, Godlinski D, Simchi A and Firouzdor V (2007) Mater Sci Eng A (in press)
8. Imgrund F, Rota A, Prtzoldt F, Simchi A (2007) Int. J. Adv Manuf Technol 33:176
9. Simchi A, Petzoldt F, Hartwig T (2005) In: Proc. of Euro PM2005 Conference and Congress, vol 2. European Powder Metallurgy Association (EPMA), Shrewsbury, UK, p 357
10. Pest A, Petzoldt F, Eifert H, Veltl G, Hartwig T, German RM (1996) In: Proc. of Powder Metallurgy and Technology World Congress. Metal Powder Industries Federation (MPIF), vol 5, part 19. Granada, Spain, p 171
11. Liu ZY, Loh NH, Khor KA, Tor SB (2000) Mater Sci Eng 293A:46
12. Varez A, Levnfeld B, Torralba JM, Matula G, Dobrzanski LA (2004) Mater Sci Eng 366A:318
13. ASM Metals Handbook, 9th edn., vol 9 (1985) ASM International, Metals Park, OH, p 282
14. Sindo K (2002) Welding metallurgy, 2nd edn. John Wiley & Sons, Inc., Publication
15. Porter DA, Easterling KE, Phase (1983) Transformations in meals and alloys. Van Nostrand Reinhold Co. Ltd., Berkshire, England, p 89
16. Shewmon P (1989) Diffusion in solids, 2nd edn. TMS Publication, p 132
17. Shu GJ, Hwang KS, Pan YT (2006) Acta Mater 54:1335
18. Tandon R, German RM (1998) Inter J Powder Metall 34:40